Hydrogenated ZnO Core–Shell Nanocables for Flexible Supercapacitors and Self-Powered Systems

Peihua Yang,[†] Xu Xiao,[§] Yuzhi Li,[†] Yong Ding,[‡] Pengfei Qiang,[†] Xinghua Tan,[†] Wenjie Mai,[†,‡,*] Ziyin Lin,[‡] Wenzhuo Wu,[‡] Tianqi Li,[§] Huanyu Jin,[§] Pengyi Liu,[†] Jun Zhou,[§] Ching Ping Wong,[‡] and Zhong Lin Wang[‡,⊥,*]

[†]Department of Physics and Siyuan Laboratory, Jinan University, Guangzhou, Guangdong 510632, China, [‡]School of Materials Science and Engineering, Georgia Institute of Technology, Atlanta, Georgia 30332, United States, [§]Wuhan National Laboratory for Optoelectronics (WNLO), and College of Optoelectronic Science and Engineering, Huazhong University of Science and Technology (HUST), Wuhan 430074, China, and [⊥]Beijing Institute of Nanoenergy and Nanosystems, Chinese Academy of Sciences, Beijing 100085, China

ABSTRACT Although MnO_2 is a promising material for supercapacitors (SCs) due to its excellent electrochemical performance and natural abundance, its wide application is limited by poor electrical conductivity. Inspired by our results that the electrochemical activity and electrical conductivity of ZnO nanowires were greatly improved after hydrogenation, we designed and fabricated hydrogenated single-crystal ZnO@amorphous ZnO-doped MnO_2 core–shell nanocables (HZM) on carbon cloth as SC electrodes, showing excellent performance such as areal capacitance of 138.7 mF/cm^2 and specific capacitance of 1260.9 F/g. Highly flexible all-solid-state SCs were subsequently assembled with these novel HZM electrodes using polyvinyl alcohol/LiCl electrolyte. The working devices achieved very high total areal capacitance of 26 mF/cm^2 and retained 87.5% of the original capacitance even after 10 000 charge/discharge cycles. An integrated power pack incorporating series-wound SCs and dye-sensitized solar cells was demonstrated for stand-alone self-powered systems.

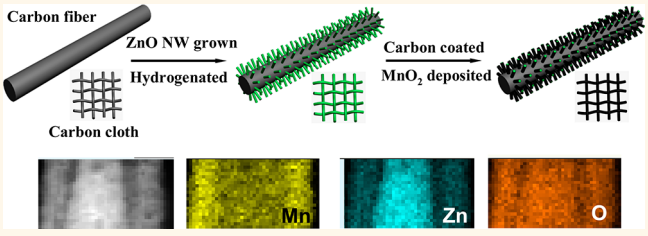

KEYWORDS: supercapacitors · hydrogenation · core–shell · flexible · self-powered · ZnO

Specific energy storage devices possessing characteristics of flexibility, light weight, and even safety may meet the large proliferation of consumer electronics. Among various emerging energy storage technologies, supercapacitors (SCs), also named electrochemical capacitors (ECs), with combined high power and high energy density, have attracted much attention and will be a promising candidate energy source.[1] Compared with liquid electrolytes SCs, all-solid-state SCs have many advantages, such as portability, environmental friendliness, and stability, which can enrich the application area of SCs.[2−7] According to the mechanism of charge storage, SCs can be classified as two kinds: electrical double-layer capacitors (EDLCs), whose charges are adsorbed electrostatically at the electrode/electrolyte interface, typically are based on carbon materials; pseudocapacitors, which store energy by redox reactions on electrode materials, are usually based on conducting polymers and transition metal oxides.[8] In fact, pseudocapacitors have higher specific capacitance than conventional EDLCs due to their fast and reversible redox reaction, so many efforts, including ours in this work, have been focused on further improving pseudocapacitors.

Compared to other transition metal oxides (RuO_x,[9] CoO_x,[10,11] NiO_x,[12] and FeO_x[13,14]), manganese dioxide (MnO_2) has significant superiorities such as low cost, low toxicity, abundant resource, and high theoretical specific capacitance (1370 F/g).[15−18] Its poor electrical conductivity, however, limits the wide application of MnO_2. To overcome this problem, several strategies have been proposed, for instance, incorporating MnO_2 with carbon-based materials such as graphene[19−21] or graphene oxide[22] and carbon nanotubes (CNTs),[18,23,24] and core–shell structures (Co_3O_4@MnO_2,[25] SnO_2@MnO_2,[26] WO_{3-x}@Au@MnO_2,[27] Zn_2SnO_4@MnO_2,[28] *etc.*). Recently, Jiang *et al.* reported MnO_2 nanowires/mesoporous carbon/MnO_2 nanoparticle hybrid nanowires, which significantly

* Address correspondence to wenjiemai@gmail.com, zlwang@gatech.edu.

Received for review December 31, 2012 and accepted January 31, 2013.

Published online February 01, 2013
10.1021/nn306044d

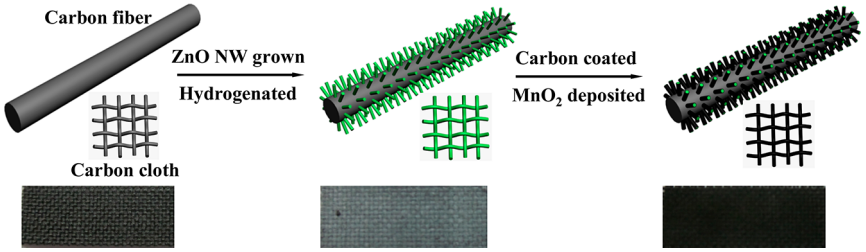

Figure 1. Schematic illustrating the synthesis procedure of HZM core/shell nanostructure on carbon cloth and the corresponding sample photos.

improved the conductivity of metal oxide materials.[29] MnO_2 in this unique structure was efficiently utilized with the assistance of the highly conductive mesoporous carbon shell. Li *et al.* designed and synthesized novel MnO_2/Mn/MnO_2 sandwich-structured nanotube arrays with high supercapacitor performance.[30] The special sandwich-structured nanotube architecture allowed highly efficient utilization of MnO_2 for charge storage with facilitated transport of ions and electrons, resulting in excellent electrochemical performance. Despite all of these achievements, enhancing the MnO_2 electrode conductivity still remains a challenge.

Zinc oxide (ZnO) nanomaterials, owing to their special chemical and physical properties, and many technical advantages such as low cost, easy fabrication, and cleanroom compatibility, are widely studied in electronics and piezotronics devices,[31,32] strain sensors,[33,34] surface switches,[35] and photocatalysis.[36] Motivated by the idea that hydrogenation of metal oxides can greatly improve its electrochemical activity and electrical conductivity,[37] here, we designed and fabricated a novel hybrid architecture by easily coating MnO_2 on hydrogenated zinc oxide nanowires (HZnO) grown on flexible carbon cloth. During the procedure, ZnO was found to be doped into the MnO_2 spontaneously. Since HZnO had improved free carrier concentration and better electrical stability, they could be a good scaffold for MnO_2 loading. Moreover, the conductive carbon cloth could serve as a lightweight and flexible current collector. Hydrogenated single-crystal ZnO@amorphous ZnO-doped MnO_2 core−shell nanocable (HZM) electrodes exhibited high electrochemical performance, and all-solid-state SCs were fabricated with these novel HZM electrodes using a polyvinyl alcohol (PVA)/LiCl neutral electrolyte *via* a simple and low-cost method. The fabricated HZM-based all-solid-state SCs exhibited many advantages in performance such as high capacitance, high flexibility, long lifetime, and low leakage current. In addition, the SCs integrated with dye-sensitized solar cells (DSSCs) could serve as a switchable power pack that is able to store energy as sunlight illuminates and light up commercial light-emitting diodes (LEDs) as light turns off, demonstrating the potential broad applications of SCs as a power pack for stand-alone self-powered systems.

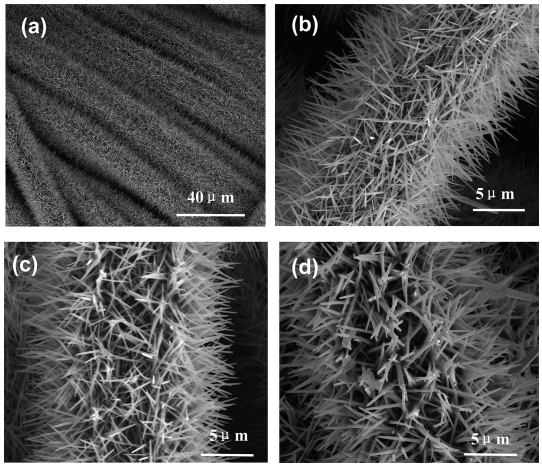

Figure 2. (a,b) SEM images of HZnO (hydrogenated ZnO nanowires grown on carbon cloth). (c) SEM image of HZC (HZnO coated with a layer of carbon). (d) SEM image of HZM (HZC deposited with a layer of MnO_2).

RESULTS AND DISCUSSION

The general electrode fabrication procedure is schematically illustrated in Figure 1. Initially, aligned and ordered ZnO nanowires (NWs) were grown on carbon cloth using a wet chemical method. The obtained ZnO NWs were about 100−200 nm in diameter and 4.5−7 μm in length (Figure 2a,b). Hydrogenation of the ZnO NWs in a commercial tube furnace improved the electrical properties of ZnO. The uniform hydrogenated ZnO NWs were then soaked in a glucose aqueous solution and subsequently annealed in Ar gas. An amorphous carbon formed and served as a reducing agent for the deposition of MnO_2 *via* the following reaction at room temperature[38,39]

$$4MnO_4^- + 3C + H_2O = 4MnO_2 + CO_3^{2-} + 2HCO_3^- \quad (1)$$

As shown in Figure 2c,d, the ZnO NWs became slightly longer in length and larger in diameter after depositions of the carbon layer and a subsequent deposition of MnO_2 layer; however, the NW morphology was preserved uniformly.

Figure 3a and Figure S1a in Supporting Information show a typical scanning transmission electron microscopy (STEM) image of an individual HZM nanocable in which a thin shell (~30 nm) uniformly covers the

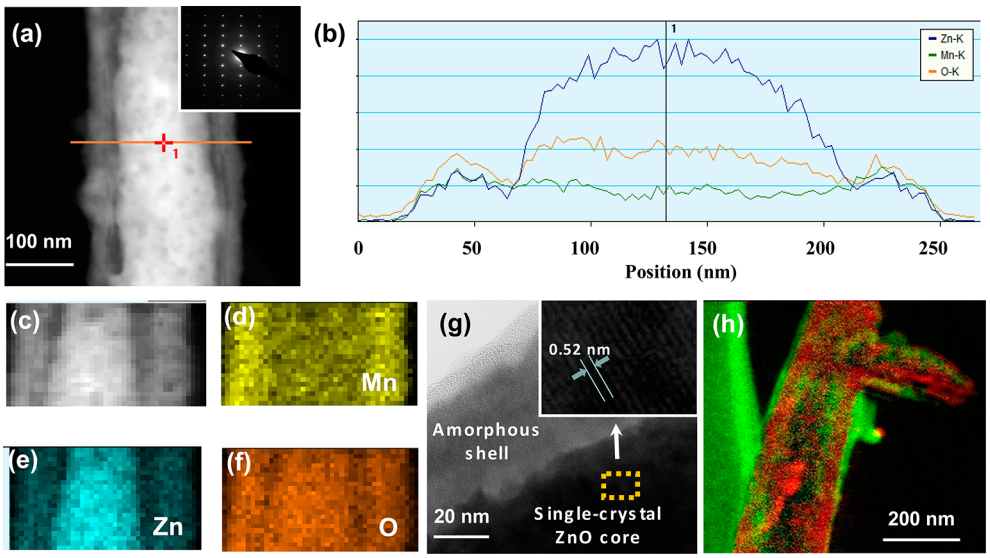

Figure 3. (a) STEM image of HZM core/shell nanostructure. Inset is SAED pattern of HZM nanocable, showing only a set of diffraction patterns from ZnO and suggesting the single-crystal ZnO core and amorphous shell. (b) EDS line scan curves showing Zn, Mn, and O element profiles across the HZM core/shell nanocable indicated in (a). (c) STEM image of a select area. (d–f) EDS element mapping images from the same area as in (c). EDS mapping images and line scan curves both indicated two elements (Zn and O) were in the core, and three elements (Mn, Zn, and O) were in the shell. (g) HRTEM image of the HZM core/shell nanocable, confirming the single-crystal ZnO core and amorphous shell. Inset image is from an enlarged area in (g), showing the 0.52 nm distance between (0001) planes and [0001] growth direction of the ZnO core. (h) EELS mapping image showing Mn (red) and C (green) elements. The EELS mapping image indicated that Mn was in the shell (consistent with EDS mapping), and C was negligible in the HZM nanocable. Green rectangular area with a protruding green dot on the HZM nanocable was carbon absorption induced by a previous STEM EDS mapping procedure.

surface of the HZnO nanowire. The corresponding selected area electron diffraction (SAED) pattern (inset of Figure 3a) suggested the single-crystal structure of the HZnO core and its [0001] growth direction. The amorphous shell was double confirmed by an electron diffraction pattern, in which no other diffraction peaks were observed besides those from ZnO (inset in Figure 3a) and random atom arrangement in high-resolution transmission electron microscopy (HRTEM) (Figure 3g). The enlarged HRTEM image of the core in the rectangular area of Figure 3g is shown in its inset, and the (0001) atomic plane spacing was measured to be 0.52 nm. Energy-dispersive X-ray spectrometry (EDS) mapping analysis of elements Mn, Zn, and O (shown in Figure 3d–f, respectively) from a select area of a single hybrid nanocable (Figure 3c) confirmed the HZM core–shell structure. EDS line scanning (indicated by a line in Figure 3a) of Zn, Mn, and O across the HZM nanowire could better illustrate the core–shell configuration (shown in Figure 3b): the profile of Zn showed a broad peak, which was located at the center of the profile, while the profile of Mn showed higher intensity on both sides. Analysis of the data indicated that the diameter of the HZnO core and the total outer diameter of the composite nanocable were about 150 and 225 nm, respectively, in accordance with the STEM image (Figure 3a).

It was worthy to point out that the Zn signal was observed from the shell structure, reflected from both EDS mapping and line scanning. The reason for this is explained in the following. During the annealing process, carbon could convert the ZnO in contact with itself to Zn metal, which was more volatile than the oxide, so the surface of ZnO nanowires was no longer as smooth as before annealing. Vaporized zinc atoms diffused into the remaining carbon shell, and sometimes it generated a tiny gap between the ZnO core and the carbon shell (Figure S1b). Subsequently, when the sample was removed from Ar atmosphere and placed in ambient conditions, the Zn atoms embedded in the outer carbon layer were unavoidably oxidized to ZnO again. As the outer carbon layer reacted with $KMnO_4$, it generated an amorphous ZnO-doped MnO_2 shell (Figure S1c). XPS data (Figures 4 and S2) showed that Mn $2p_{3/2}$ and Mn $2p_{1/2}$ peaks were located at *ca.* 642.2 and 653.8 eV, suggesting the element Mn in the sample was present in the chemical state of Mn^{4+}. The Zn $2p_{3/2}$ and Zn $2p_{1/2}$ lines were found at the binding energies of about 1021.3 and 1044.4 eV, indicating the existence of ZnO. The electron energy loss spectroscopy (EELS) mapping image is shown in Figure 3h, indicating Mn (red color) in the shell (consistent with EDS data in Figure 3b,d). The element C (green color) was negligible in the HZM nanocable, implying that the carbon already fully reacted with $KMnO_4$. Green rectangular area with a protruding green dot on the HZM nanocable was carbon absorption induced by e-beam during the previous EDS mapping procedure. Zn and O signals were weak and unclear in this EELS mapping, and as such, they were not recorded. Therefore, this novel

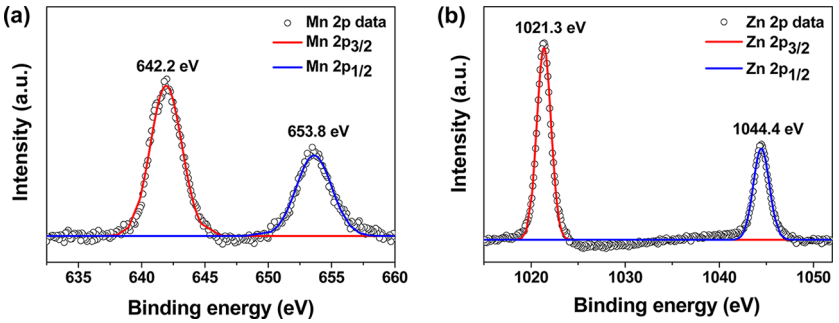

Figure 4. XPS spectra of (a) Mn 2p and (b) Zn 2p collected from the HZM core/shell nanocable. Mn $2p_{3/2}$ and Mn $2p_{1/2}$ peaks were located at *ca.* 642.2 and 653.8 eV, suggesting Mn^{4+} ions. The Zn $2p_{3/2}$ and Zn $2p_{1/2}$ lines were found at the binding energies of about 1021.3 and 1044.4 eV, which were consistent with the values reported for ZnO.

nanostructure shown in Figure 3a was finally identified and noted as a single-crystal ZnO@amorphous ZnO-doped MnO_2 core−shell nanocable. The synergistic enhancement of the electromechanical performance of this novel core−shell structure might originate from three aspects: first, the thin MnO_2 shell was in favor of the fast redox reaction, which would obtain high specific capacitance; second, the HZnO core nanowire served as a fast path for electron transport, which would support high-power density; finally, the ZnO doping in MnO_2 might improve the electrical conductivity and electrochemical performance of MnO_2. Unfortunately, we actually cannot find a method to remove the ZnO core but preserve the ZnO that was doped in the shell; therefore, we cannot directly compare the electrical conductivity and electrochemical performance between the ZnO-doped MnO_2 shell and pristine MnO_2.

Gogotsi and Simon had pointed out that a true performance metric in electrochemical energy storage should include the device components,[40] so we replaced gravimetric with arealmetric and volumetric. To explore the electrochemical properties of HZnO electrodes, electrochemical measurements were conducted in a three-electrode electrochemical cell with a graphite rod counter electrode, a Ag/AgCl reference electrode, and a 0.5 M Na_2SO_4 aqueous electrolyte. Figure 5a shows the cyclic voltammetry (CV) curves of untreated ZnO, air-annealed ZnO (AZnO), and HZnO electrodes collected at the scan rate of 100 mV/s. The nearly rectangular shaped curves suggested that ZnO NWs mainly work as an EDLC. The CV area of the HZnO electrode was much larger than AZnO and ZnO electrodes, suggesting a larger specific capacitance. The electrochemical performance of differently treated ZnO samples was further studied by the galvanostatic charge/discharge measurement. Typical galvanostatic charge/discharge curves of different ZnO electrodes collected at a current density of 0.05 mA/cm^2 are shown in Figure 5b. The charge/discharge curve of the HZnO electrode was symmetric and much prolonged over the ZnO and AZnO electrodes. The areal capacitance of the HZnO sample was significantly higher than those for ZnO and AZnO electrodes. For instance, the areal capacitance of the HZnO electrode achieved 1.38 mF/cm^2 at a current density of 0.05 mA/cm^2, which was approximately a 3- and 5-fold enhancement compared with the AZnO (0.46 mF/cm^2) and ZnO (0.27 mF/cm^2) electrodes, respectively. This areal capacitance of HZnO was much improved than other ZnO-based (0.15 mF/cm^2 at 0.03 mA/cm^2) SC[41] and was also comparable with the value reported in the literature for carbon-based (0.4−2 mF/cm^2) SCs.[42,43] Additionally, it showed a smaller IR drop (0.027 V), confirming the good electrical conductivity of the HZnO electrode. According to the electrochemical impedance spectroscopy (EIS) curves in Figure 5c, the equivalent series resistance (ESR) was only 2.22 Ω for HZnO samples of 1 cm^2 area, much lower than 3.83 Ω for AZnO and 3.77 Ω for ZnO, further proving the good electrical properties of the HZnO that resulted from the hydrogenation.

To investigate the underlying mechanism for the enhanced electrical properties of ZnO by hydrogenation, Mott−Schottky (MS) measurements were conducted. This method was based on the Schottky barrier formation between the semiconductor material and an electrolyte.[44] The variation of the differential capacitance (C_s) of the space charge layer was measured as a function of the applied potential. As shown in Figure 5d, all ZnO samples exhibited a positive slope, indicating n-type semiconductor character. Carrier densities (N_d) of ZnO samples were calculated by the following equation[45]

$$N_d = \frac{2}{\varepsilon\varepsilon_0 e A^2} \frac{dV}{dC_s^{-2}} \quad (2)$$

where ε is the relative dielectric constant of ZnO (usually 8.5), ε_0 is the permittivity of vacuum, V is the potential applied at the electrode, and A is the area in contact with the electrolyte. The carrier densities of the HZnO, AZnO, and ZnO NWs were calculated to be 2.65×10^{20}, 1.86×10^{18}, and 7.04×10^{17} cm^{-3}, respectively. Although the MS equation was derived from a planar model, these results are still qualitatively comparable as these electrodes have similar morphology

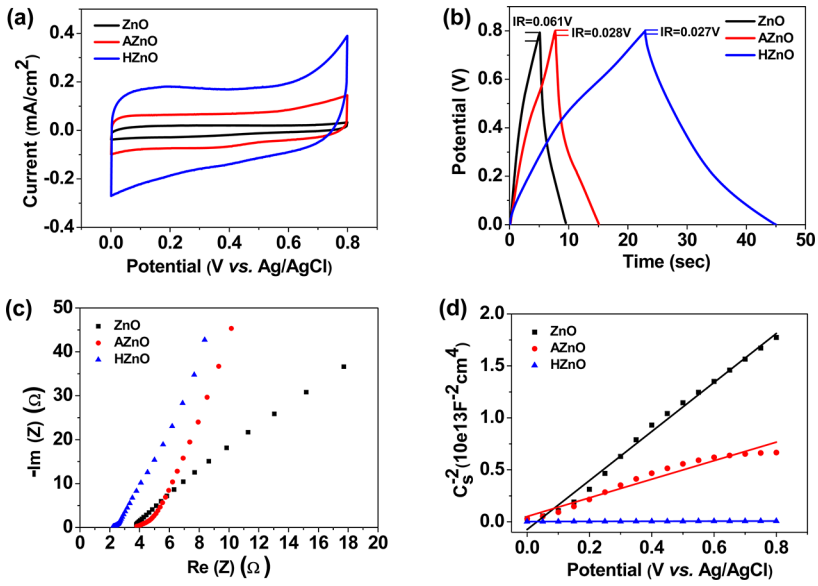

Figure 5. (a) CV curves for ZnO, AZnO, and HZnO at a scan rate of 100 mV/s. (b) Galvanostatic charge/discharge curves of ZnO, AZnO, and HZnO collected at a current density of 0.05 mA/cm^2. (c) Nyquist plots and (d) Mott–Schottky plots of ZnO, AZnO, and HZnO electrodes with an area of 1 cm^2.

and surface area. The significant enhancement in the carrier density, which is over 2 orders of magnitude, could be clearly attributed to the hydrogen insertion. The low-energy oxygen vacancies that might be formed in high concentrations would be neutral and electrically inactive in n-type ZnO; however, the substitutional hydrogen atoms for the oxygen vacancies acted as shallow donors.[46] The improved electrical conductivity and stability indicated that hydrogen played an important role in n-type conduction as the donor. This result was also in accord with a previous report by Lu *et al.*[37]

The aforementioned experimental results confirmed that HZnO NWs had better electrochemical and electrical properties, which enabled them to serve as effective support for other capacitive materials to form composite structures. Here, HZM nanocables were synthesized on carbon cloth *via* a self-limiting process (see Methods).

To demonstrate the electrochemical performance of the composite structures, the electrochemical properties of nanocable samples were first characterized in three-electrode ECs with CV, galvanostatic charge/discharge, and EIS measurements in 0.5 M Na_2SO_4 aqueous solution. The CV curves of untreated ZnO/ZnO-doped MnO_2 (ZM), air-annealed ZnO/ZnO-doped MnO_2 (AZM), and HZM electrodes collected at the scan rate of 100 mV/s are shown in Figure 6a. The HZM electrode exhibited a quasi-rectangular shape and a much more enhanced capacitive current density. Figure 6b shows the galvanostatic charge/discharge curves of different nanocable electrodes collected at a current density of 1 mA/cm^2. The negligible IR drop (0.019 V) was even smaller than HZnO electrode discharged at 0.05 mA/cm^2, benefitting from the synergistic effect of improved electrical performance of hydrogenated ZnO core and ZnO-doped MnO_2 shell. The areal capacitance (C_a) of the electrode was calculated by the following equation

$$C_a = \frac{I\Delta t}{S\Delta E} \quad (3)$$

where I is the discharge current, Δt is the discharge time, ΔE is the potential window during the discharge process (subtract the IR drop), and S is the effective electrode area. The areal capacitance of HZM electrodes were as high as 138.7 mF/cm^2 at a current density of 1 mA/cm^2, which was 1.6 and 2.8 times those of AZM (88.2 mF/cm^2) and ZM (49.3 mF/cm^2) electrodes (Figure 6c), respectively. Remarkably, this value is also higher than the values reported for other manganese oxide composites, such as TiN@MnO_2 coaxial arrays (~41 mF/cm^2 at 0.12 mA/cm^2),[47] PEDOT@MnO_2 nanoparticles (~62 mF/cm^2 at 5 mA/cm^2),[48] SnO_2@MnO_2 nanowires (~64 mF/cm^2 at 0.08 mA/cm^2),[26] hydrogenated TiO_2@MnO_2 nanowires (~70 mF/cm^2 at 2 mA/cm^2),[49] and WO_{3-x}@Au@MnO_2 nanowires (~105 mF/cm^2 at 0.06 mA/cm^2),[27] and even comparable to graphene sheets/Mn_3O_4 composites (~242 mF/cm^2 at 1 mA/cm^2).[50] The specific capacitance was calculated as 1260.9 F/g since the loading of MnO_2 was 0.11 mg/cm^2 determined by inductively coupled plasma atomic emission spectroscopy. Furthermore, HZM electrodes of 1 cm^2 area showed very low ESR values (2.74 Ω) in Figure 6d, suggesting that the HZM electrodes have very small resistance with good ion response at high-frequency ranges. The very low ESR value further confirmed that the HZnO NWs could indeed act as a good substrate for MnO_2 loading.

An all-solid-state symmetric flexible SC was assembled with two HZM electrodes using a solid

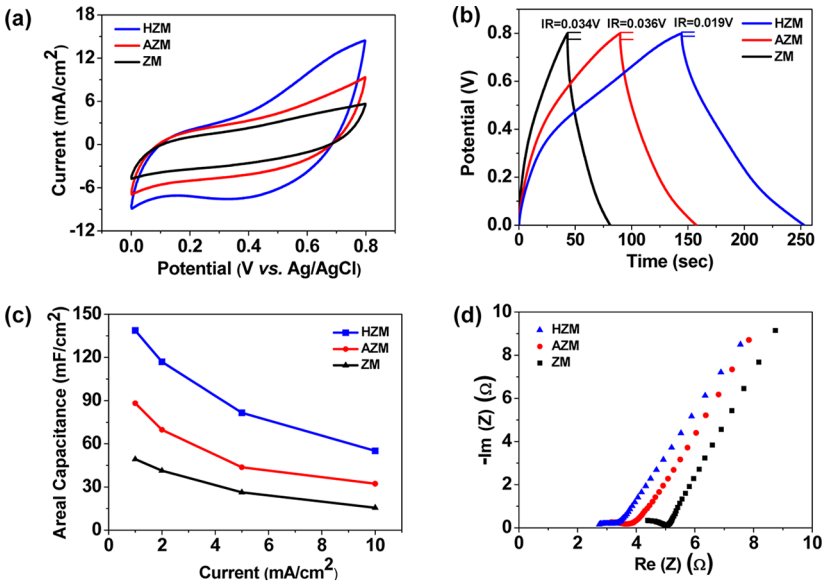

Figure 6. (a) CV curves for ZM, AZM, and HZM electrodes at a scan rate of 100 mV/s. (b) Galvanostatic charge/discharge curves of ZM, AZM, and HZM collected at a current density of 1 mA/cm^2. (c) Areal capacitances of the ZM, AZM, and HZM electrodes measured as a function of current density. (d) Nyquist plots for ZM, AZM, and HZM electrodes with an area of 1 cm^2.

PVA/LiCl electrolyte (Figure 7a). The CV curves in Figure 7b suggested that the SC could be bent and twisted without affecting the device performance much, showing good flexibility and stability. Galvanostatic charge/discharge tests were also performed with different current densities with a voltage window of 0−0.8 V (Figure 7c). The linear and symmetric curves revealed the good capacitive characteristic of the solid-state SC. The total areal capacitance of the device was nearly 26 mF/cm^2 (or 325 mF/cm^3) at a current density of 0.5 mA/cm^2, which was higher than other solid-state devices reported previously, for instance, laser scribing graphene (~1.84 mF/cm^2 at 0.82 mA/cm^2)[51] and bacterial nanocellulose/carbon nanotubes (~20 mF/cm^2 at 0.4 mA/cm^2),[6] and even on the verge of carbon nanotubes papers (~31 mF/cm^2 at 0.46 mA/cm^2).[52] Figure S3a showed the CV curves of the symmetric SC measured at scan rates ranging from 10 to 100 mV/s. These CV curves exhibited nearly rectangular shapes. The cycle life of the SC was tested through a cyclic charge/discharge process at a current density of 0.5 mA/cm^2, which is shown in Figure 7d. After 10 000 cycles, over 87.5% capacitance was maintained, demonstrating the excellent electrochemical performance of this HZM nanocable electrode material. The Coulombic efficiency (η) of the SC was characterized by a charge/discharge process according to

$$\eta = \frac{\Delta t_d}{\Delta t_c} \quad (4)$$

where Δt_d and Δt_c represent the discharge and charge times, respectively. The Coulombic efficiency nearly exceeded 90% (Figure 7d), implying good charge/discharge reversibility for the solid-state SC. Potentiostatic EIS measurements were performed after first and 10 000th cycles to evaluate the internal resistance change during the cycling charge/discharge test (Figure S3b). An insignificant shift of ESR was observed from 5.9 to 9.0 Ω. The increase of charge transfer resistance might be caused by the distortion of charge transport pathway. Energy density (E) and power density (P) are two key factors for evaluating the application of SCs, which can be calculated as

$$E = \frac{CV^2}{2U} \quad (5)$$

$$P = \frac{E}{t} \quad (6)$$

where C is total capacitance of the device, V is the cell voltage, U is the device volume, and t is the discharge time. A power density of 2.44 mW/cm^3 and an energy density of 0.04 mWh/cm^3 were achieved. In particular, the energy density of our SC was higher than that of the other solid-state SCs (shown in Figure 7e), such as CNT-based SCs (0.008 mWh/cm^3)[52] and MnO_2-coated ZnO NWs (0.005 mWh/cm^3).[41]

As efficient energy storage devices, SCs should be able to not only drive electrical components but also store energy from various other energy sources, especially intermittent sources. Solar energy is probably the most clean and renewable energy in the world, but it is always limited by time, location, and weather. Integrating dye-sensitized solar cells (DSSCs) with energy storage devices such as SCs and batteries may offer a promising solution to build stand-alone self-powered systems,[53−55] which potentially break the limitations of time, location, and weather. Specially, to demonstrate the potential applications of our newly fabricated all-solid-state SCs, we designed a stand-alone

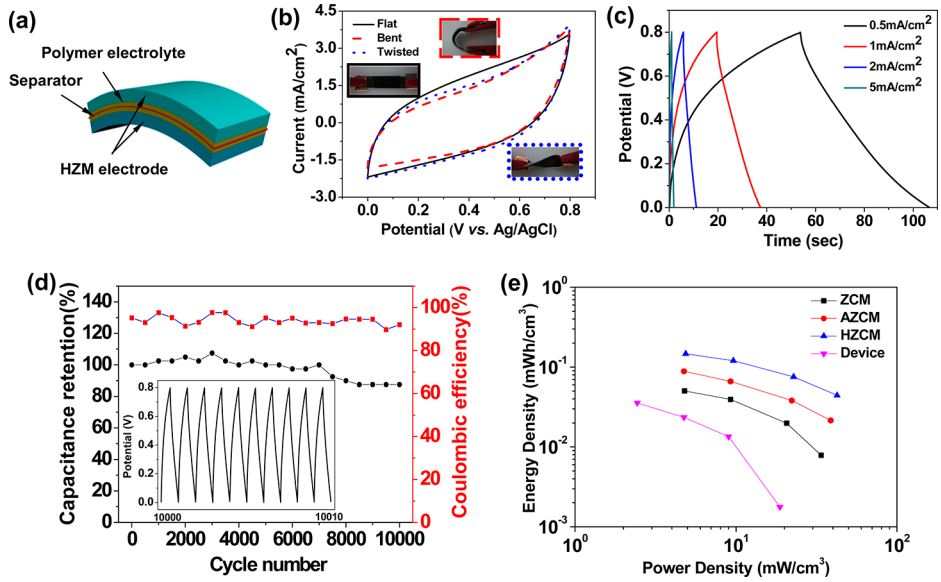

Figure 7. (a) Schematic diagram of a solid-state HZM SC, with a separator and PVA/LiCl polymer as the electrolyte. (b) CV curves collected at a scan rate of 100 mV/s for the HZM SC device under flat, bent, and twisted conditions, indicating the flexibility of HZM SC devices. Insets are the photos of the device under the corresponding test conditions. (c) Galvanostatic charge/discharge curves collected at different current densities for the HZM SC device. (d) Cycle performance and Coulombic efficiency of the HZM SC device measured at a current density of 0.5 mA/cm^2. The inset showed the galvanostatic charge/discharge curve after 10 000 cycles. These results suggest good stability and long lifetime of devices. (e) Ragone plots of the ZM, AZM, HZM electrodes, and HZM-based SC device.

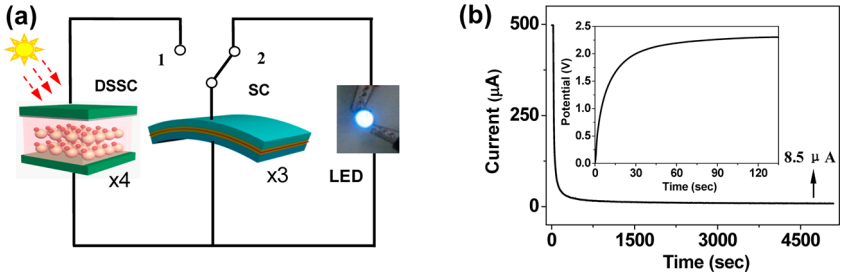

Figure 8. (a) Schematic of a stand-alone self-powered system consisting of four series-wound DSSCs, three series-wound flexible SCs, and one LED. (b) Leakage current curve of three series-wound SCs charged at 0.5 mA to a potential of 2.4 V and kept at 2.4 V for 5000 s, indicating small leakage current. Inset is the voltage profile for three SCs in series when being charged by four DSSCs in series.

self-powered system consisting of DSSCs, SCs, and LEDs. Simple schematic view of a self-powered system is illustrated in Figure 8a. The switchable power pack in this system consisted of an environmental energy-harvesting module (four series-wound homemade DSSCs) and an energy storage module (three series-wound SCs). The photovoltaic performance of a DSSC cell was measured under the illumination of AM 1.5 (100 mW/cm^2) by recording the current density/voltage response (Figure S4). When sunlight was available, the switch was set at position "1", so the DSSCs harvested solar energy and stored the energy in the SCs. After 120 s charging under the illumination, the voltage of three series-wound SCs reached approximately 2.3 V (inset in Figure 8b). When the solar source was turned off and the room became dark, the switch was then placed to position "2", and the charged SCs could drive a commercial blue LED to illuminate (Figure S5b). A red LED in this stand-alone self-powered system could be lighted up for more than 30 min by three series-wound SCs, which were previously charged by four series-wound DSSCs for 2 min. Figure S5b and video S1 demonstrate that an LED was powered by three series-wound SCs. At the beginning, the LED twinkled very brightly, demonstrating the excellent power merit of SCs. Figure S5a showed the time courses of the open-circuit voltage of the series-wound SCs. It gently underwent a self-discharge course; furthermore, the SC devices showed an output of ~1.5 V after 40 min. On the level of practical application, leakage current of the devices is critical. As shown in Figure 8b, the leakage current dropped significantly at the beginning (from 0.5 mA to 68.7 μA after 100 s and to 22.8 μA after 400 s) and then gradually became stable and small (finally to only 8.5 μA after 4500 s). This value was even smaller than that of the CNT/PANI supercapacitor,[2] indicating few impurities in the electrode and electrolyte materials in the fabricated SCs. Such demonstration implied

that the stand-alone self-powered systems had potential applications in combining mobile devices and driving small electrical compounds.

CONCLUSION

In summary, we have reported the design and synthesis of a novel nanocable material, HZM with a hydrogenated single-crystal ZnO core and amorphous ZnO-doped MnO_2 shell, as well as the fabrication of a new kind of flexible all-solid-state SC configuration with two pieces of slightly separated carbon cloth grown with HZM nanocables as electrodes and PVA/LiCl gel as solid-state electrolyte. The SC devices exhibited many advantages in performance such as high capacitance, high flexibility, long lifetime, and low leakage current. The hydrogenated ZnO core with larger charge concentration and ZnO-doped MnO_2 shell with better conductivity contributed to the high performance of SCs. Our HZM flexible SCs might greatly contribute to the fundamental research and technologies of flexible energy storage devices. A potential application of the flexible solid-state SCs as a switchable power source in stand-alone self-powered systems was demonstrated, which exhibited the potential broad applications of the SCs.

METHODS

Synthesis of HZM. First, ZnO NWs were grown on carbon cloth (WOS1002, 2.5 cm × 0.7 cm × 360 μm) by a wet chemical process. Briefly, carbon cloth was first soaked in 0.5 M $KMnO_4$ for 30 min to form a seed layer. A precursor 100 mL solution was prepared with 0.015 M of zinc nitrate hexahydrate and 0.015 M of hexamethylenetetramine (HMTA) added with 4 mL of ammonia. The seeded carbon cloth substrates were dipped into the precursor solution then placed under 90 °C for 24 h. After the wet chemical process, ZnO NWs were grown on the carbon cloth. The HZnO NWs were obtained by annealing the ZnO NWs in hydrogen atmosphere at 350 °C for 3 h. ZnO NW samples were also annealed in air at 350 °C for 3 h to obtain AZnO as control samples for comparison. Second, the HZnO NWs were immersed into a 0.5 M aqueous glucose solution for 24 h. HZC samples were obtained by carbonization at 450 °C in Ar gas for 2 h. Third, MnO_2 was deposited on HZC *via* a self-limiting process.[38] Simply, 0.5 M $KMnO_4$ and 0.5 M Na_2SO_4 was mixed with equal volume. The HZC samples were immersed in the solution for 8 h at room temperature. Then the HZM was cleaned several times using deionized water. The loading mass of MnO_2 was 0.11 mg/cm^2.

Assembly of the Solid-State SC. The SC was assembled by two pieces of HZM NW electrodes with a separator (NKK TF40, 40 μm) and LiCl/PVA gel as a solid electrolyte. LiCl/PVA gel was prepared by mixing LiCl (12.6 g) and PVA (6 g) in 60 mL of deionized water and heated at 85 °C under stirring for 2 h. Two electrodes and separator were soaked in the gel for about 5 min and then assembled together. The device was kept at 60 °C for 12 h to remove excess water in the electrolyte. After the gel electrolyte became hard, the thickness of the device was around 0.8 mm. The SC was sealed with tape to prevent absorbing water.

Material Characterization and Electrochemical Measurement. The structural properties of electrode materials were characterized by field-emission SEM (FEI Sirion 2000), TEM (FEI TECNAI F30) equipped with an energy-dispersive X-ray spectroscopy (EDS) detector, and electron energy loss spectroscopy (EELS) detector, X-ray photoelectron spectroscope (XPS, Thermo K-alpha). The loading mass of MnO_2 was analyzed by inductively coupled plasma atomic emission spectroscopy (OPTIMA 2000DV). The electrochemical properties of the products were investigated with cyclic voltammetry (CV) and chronopotentiometry measurements employing a CHI 660D electrochemical workstation (Chenhua, Shanghai) and VersaSTAT 3 (Princeton Applied Research), and the electrochemical impedance spectroscopy (EIS) was measured by an Autolab PGSTAT302N at a frequency ranging from 100 mHz to 10 kHz with a potential amplitude of 10 mV. The photoelectric conversions were characterized by recording voltage−current curves with a computerized digital multimeter (Keithley 2601A). An AM 1.5 solar stimulator (Abet Model 11000) calibrated to 100 mW/cm^2 by a reference Si solar cell was used in photovoltaic characteristic experiments. Mott−Schottky plots were measured at a frequency of 10000 Hz based on ZnO samples grown on FTO substrates. The cycle life was measured through a battery test system (Neware BTS). For a single electrode test, a piece of electrode (~0.7 cm × 1.5 cm, effective area ~1 cm^2) was dipped into 0.5 M Na_2SO_4 solution at room temperature. Ag/AgCl reference electrode and graphite rod counter electrode were used in the measurement.

Conflict of Interest: The authors declare no competing financial interest.

Acknowledgment. Authors thank Dr. Z.-H. Lin and Dr. Y. Yang from Georgia Tech, T. Zhai and Prof. Y.X. Tong from Zhongshan University, Dr. X. Cai and Prof. S.Z. Tan from Jinan University for technical assistance and helpful discussions. P.H.Y., X.H.T., and Y.Z. L. thank Jinan University student training programs for financial support (Grant Nos. 1210559068 and 2012Science18). W.J.M. thanks the National Natural Science Foundation of China (Grant No. 51102115), the Specialized Research Fund for the Doctoral Program of Higher Education of China (Grant No. 20104401120005), the Key Project of Chinese Ministry of Education (Grant No. 211208), the China Scholarship Council (Grant No. 201206785006), and the Fundamental Research Funds for the Central Universities (Grant No. 21612109) for financial support. Z.L.W. thanks the Knowledge Innovation Program of the Chinese Academy of Sciences (KJCX2-YW-M13).

Supporting Information Available: Assembly of the DSSCs, TEM images for HZ and HZM, more XPS analysis data of HZM, self-discharge curve of the SC, more EIS data, schematic of the DSSCs, DSSC data, more electrical and electrochemical data for ZnO, AZnO, HZnO, ZM, AZM, and HZM electrodes, and a video of lighting up a red LED by three series-wound SCs. This material is available free of charge *via* the Internet at http://pubs.acs.org.

REFERENCES AND NOTES

1. Simon, P.; Gogotsi, Y. Materials for Electrochemical Capacitors. *Nat. Mater.* **2008**, *7*, 845–854.
2. Meng, C.; Liu, C.; Chen, L.; Hu, C.; Fan, S. Highly Flexible and All-Solid-State Paperlike Polymer Supercapacitors. *Nano Lett.* **2010**, *10*, 4025–4031.
3. Yuan, L.; Xiao, X.; Ding, T.; Zhong, J.; Zhang, X.; Shen, Y.; Hu, B.; Huang, Y.; Zhou, J.; Wang, Z. L. Paper-Based Supercapacitors for Self-Powered Nanosystems. *Angew. Chem., Int. Ed.* **2012**, *51*, 4934–4938.
4. Xiao, X.; Ding, T.; Yuan, L.; Shen, Y.; Zhong, Q.; Zhang, X.; Cao, Y.; Hu, B.; Zhai, T.; Gong, L.; *et al.* WO_{3-x}/MoO_{3-x} Core/Shell Nanowires on Carbon Fabric as an Anode for All-Solid-State Asymmetric Supercapacitors. *Adv. Energy Mater.* **2012**, *2*, 1328–1332.
5. Yuan, L.; Lu, X.-H.; Xiao, X.; Zhai, T.; Dai, J.; Zhang, F.; Hu, B.; Wang, X.; Gong, L.; Chen, J.; *et al.* Flexible Solid-State Supercapacitors Based on Carbon Nanoparticles/MnO_2 Nanorods Hybrid Structure. *ACS Nano* **2011**, *6*, 656–661.
6. Kang, Y. J.; Chun, S.-J.; Lee, S.-S.; Kim, B.-Y.; Kim, J. H.; Chung, H.; Lee, S.-Y.; Kim, W. All-Solid-State Flexible Supercapacitors Fabricated with Bacterial Nanocellulose Papers, Carbon Nanotubes, and Triblock-Copolymer Ion Gels. *ACS Nano* **2012**, *6*, 6400–6406.

7. Xiao, X.; Li, T.; Yang, P.; Gao, Y.; Jin, H.; Ni, W.; Zhan, W.; Zhang, X.; Cao, Y.; Zhong, J.; *et al.* Fiber-Based All-Solid-State Flexible Supercapacitors for Self-Powered Systems. *ACS Nano* **2012**, *6*, 9200–9206.
8. Conway, B. E. *Electrochemical Supercapacitor: Scientific Fundmentals and Technological Applications*; Kluwer Academic/Plenum Publishers: New York, 1999.
9. Hu, C.-C.; Chang, K.-H.; Lin, M.-C.; Wu, Y.-T. Design and Tailoring of the Nanotubular Arrayed Architecture of Hydrous RuO_2 for Next Generation Supercapacitors. *Nano Lett.* **2006**, *6*, 2690–2695.
10. Kung, C.-W.; Chen, H.-W.; Lin, C.-Y.; Vittal, R.; Ho, K.-C. Synthesis of Co_3O_4 Nanosheets *via* Electrodeposition Followed by Ozone Treatment and Their Application to High-Performance Supercapacitors. *J. Power Sources* **2012**, *214*, 91–99.
11. Yuan, C.; Yang, L.; Hou, L.; Shen, L.; Zhang, X.; Lou, X. W. Growth of Ultrathin Mesoporous Co_3O_4 Nanosheet Arrays on Ni Foam for High-Performance Electrochemical Capacitors. *Energy Environ. Sci.* **2012**, *5*, 7883–7887.
12. Wang, B.; Chen, J. S.; Wang, Z.; Madhavi, S.; Lou, X. W. Green Synthesis of NiO Nanobelts with Exceptional Pseudo-Capacitive Properties. *Adv. Energy Mater.* **2012**, *2*, 1188–1192.
13. Qu, Q.; Yang, S.; Feng, X. 2D Sandwich-like Sheets of Iron Oxide Grown on Graphene as High Energy Anode Material for Supercapacitors. *Adv. Mater.* **2011**, *23*, 5574–5580.
14. Xie, K.; Li, J.; Lai, Y.; Lu, W.; Zhang, Z. A.; Liu, Y.; Zhou, L.; Huang, H. Highly Ordered Iron Oxide Nanotube Arrays as Electrodes for Electrochemical Energy Storage. *Electrochem. Commun.* **2011**, *13*, 657–660.
15. Wei, W.; Cui, X.; Chen, W.; Ivey, D. G. Manganese Oxide-Based Materials as Electrochemical Supercapacitor Electrodes. *Chem. Soc. Rev.* **2011**, *40*, 1697–1721.
16. Toupin, M.; Brousse, T.; Bélanger, D. Charge Storage Mechanism of MnO_2 Electrode Used in Aqueous Electrochemical Capacitor. *Chem. Mater.* **2004**, *16*, 3184–3190.
17. Lu, X.; Zheng, D.; Zhai, T.; Liu, Z.; Huang, Y.; Xie, S.; Tong, Y. Facile Synthesis of Large-Area Manganese Oxide Nanorod Arrays as a High-Performance Electrochemical Supercapacitor. *Energy Environ. Sci.* **2011**, *4*, 2915–2921.
18. Hu, L.; Chen, W.; Xie, X.; Liu, N.; Yang, Y.; Wu, H.; Yao, Y.; Pasta, M.; Alshareef, H. N.; Cui, Y. Symmetrical MnO_2–Carbon Nanotube–Textile Nanostructures for Wearable Pseudocapacitors with High Mass Loading. *ACS Nano* **2011**, *5*, 8904–8913.
19. Fan, Z.; Yan, J.; Wei, T.; Zhi, L.; Ning, G.; Li, T.; Wei, F. Asymmetric Supercapacitors Based on Graphene/MnO_2 and Activated Carbon Nanofiber Electrodes with High Power and Energy Density. *Adv. Funct. Mater.* **2011**, *21*, 2366–2375.
20. Li, Z.; Mi, Y.; Liu, X.; Liu, S.; Yang, S.; Wang, J. Flexible Graphene/MnO_2 Composite Papers for Supercapacitor Electrodes. *J. Mater. Chem.* **2011**, *21*, 14706–14711.
21. Yu, G.; Hu, L.; Vosgueritchian, M.; Wang, H.; Xie, X.; McDonough, J. R.; Cui, X.; Cui, Y.; Bao, Z. Solution-Processed Graphene/MnO_2 Nanostructured Textiles for High-Performance Electrochemical Capacitors. *Nano Lett.* **2011**, *11*, 2905–2911.
22. Chen, S.; Zhu, J.; Wu, X.; Han, Q.; Wang, X. Graphene Oxide–MnO_2 Nanocomposites for Supercapacitors. *ACS Nano* **2010**, *4*, 2822–2830.
23. Li, X.; Wei, B. Facile Synthesis and Super Capacitive Behavior of SWNT/MnO_2 Hybrid Films. *Nano Energy* **2012**, *1*, 479–487.
24. Lee, S. W.; Kim, J.; Chen, S.; Hammond, P. T.; Shao-Horn, Y. Carbon Nanotube/Manganese Oxide Ultrathin Film Electrodes for Electrochemical Capacitors. *ACS Nano* **2010**, *4*, 3889–3896.
25. Liu, J.; Jiang, J.; Cheng, C.; Li, H.; Zhang, J.; Gong, H.; Fan, H. J. Co_3O_4 Nanowire@MnO_2 Ultrathin Nanosheet Core/Shell Arrays: A New Class of High-Performance Pseudocapacitive Materials. *Adv. Mater.* **2011**, *23*, 2076–2081.
26. Yan, J.; Khoo, E.; Sumboja, A.; Lee, P. S. Facile Coating of Manganese Oxide on Tin Oxide Nanowires with High-Performance Capacitive Behavior. *ACS Nano* **2010**, *4*, 4247–4255.
27. Lu, X.; Zhai, T.; Zhang, X.; Shen, Y.; Yuan, L.; Hu, B.; Gong, L.; Chen, J.; Gao, Y.; Zhou, J.; *et al.* WO_{3-x}@Au@MnO_2 Core–Shell Nanowires on Carbon Fabric for High-Performance Flexible Supercapacitors. *Adv. Mater.* **2012**, *24*, 938–944.
28. Bao, L.; Zang, J.; Li, X. Flexible Zn_2SnO_4/MnO_2 Core/Shell Nanocable–Carbon Microfiber Hybrid Composites for High-Performance Supercapacitor Electrodes. *Nano Lett.* **2011**, *11*, 1215–1220.
29. Jiang, H.; Yang, L.; Li, C.; Yan, C.; Lee, P. S.; Ma, J. High-Rate Electrochemical Capacitors from Highly Graphitic Carbon-Tipped Manganese Oxide/Mesoporous Carbon/Manganese Oxide Hybrid Nanowires. *Energy Environ. Sci.* **2011**, *4*, 1813–1819.
30. Li, Q.; Wang, Z.-L.; Li, G.-R.; Guo, R.; Ding, L.-X.; Tong, Y.-X. Design and Synthesis of MnO_2/Mn/MnO_2 Sandwich-Structured Nanotube Arrays with High Supercapacitive Performance for Electrochemical Energy Storage. *Nano Lett.* **2012**, *12*, 3803–3807.
31. Wang, Z. L. Progress in Piezotronics and Piezo-Phototronics. *Adv. Mater.* **2012**, *24*, 4632–4646.
32. Liang, Z.; Cai, X.; Tan, S.; Yang, P.; Zhang, L.; Yu, X.; Chen, K.; Zhu, H.; Liu, P.; Mai, W. Fabrication of n-Type ZnO Nanowire/Graphene/p-Type Silicon Hybrid Structures and Electrical Properties of Heterojunctions. *Phys. Chem. Chem. Phys.* **2012**, *14*, 16111–16114.
33. Xiao, X.; Yuan, L.; Zhong, J.; Ding, T.; Liu, Y.; Cai, Z.; Rong, Y.; Han, H.; Zhou, J.; Wang, Z. L. High-Strain Sensors Based on ZnO Nanowire/Polystyrene Hybridized Flexible Films. *Adv. Mater.* **2011**, *23*, 5440–5444.
34. Mai, W.; Liang, Z.; Zhang, L.; Yu, X.; Liu, P.; Zhu, H.; Cai, X.; Tan, S. Strain Sensing Mechanism of the Fabricated ZnO Nanowire–Polymer Composite Strain Sensors. *Chem. Phys. Lett.* **2012**, *538*, 99–101.
35. Yang, P.; Wang, K.; Liang, Z.; Mai, W.; Wang, C.-X.; Xie, W.; Liu, P.; Zhang, L.; Cai, X.; Tan, S.; *et al.* Enhanced Wettability Performance of Ultrathin ZnO Nanotubes by Coupling Morphology and Size Effects. *Nanoscale* **2012**, *4*, 5755–5760.
36. Zhang, L.; Du, L.; Cai, X.; Yu, X.; Zhang, D.; Liang, L.; Yang, P.; Xing, X.; Mai, W.; Tan, S.; *et al.* Role of Graphene in Great Enhancement of Photocatalytic Activity of ZnO Nanoparticle–Graphene Hybrids. *Physica E* **2013**, *47*, 279–284.
37. Lu, X.; Wang, G.; Xie, S.; Shi, J.; Li, W.; Tong, Y.; Li, Y. Efficient Photocatalytic Hydrogen Evolution over Hydrogenated ZnO Nanorod Arrays. *Chem. Commun.* **2012**, *48*, 7717–7719.
38. Fischer, A. E.; Pettigrew, K. A.; Rolison, D. R.; Stroud, R. M.; Long, J. W. Incorporation of Homogeneous, Nanoscale MnO_2 within Ultraporous Carbon Structures *via* Self-Limiting Electroless Deposition: Implications for Electrochemical Capacitors. *Nano Lett.* **2007**, *7*, 281–286.
39. Jin, X.; Zhou, W.; Zhang, S.; Chen, G. Z. Nanoscale Microelectrochemical Cells on Carbon Nanotubes. *Small* **2007**, *3*, 1513–1517.
40. Gogotsi, Y.; Simon, P. True Performance Metrics in Electrochemical Energy Storage. *Science* **2011**, *334*, 917–918.
41. Bae, J.; Song, M. K.; Park, Y. J.; Kim, J. M.; Liu, M.; Wang, Z. L. Fiber Supercapacitors Made of Nanowire-Fiber Hybrid Structures for Wearable/Flexible Energy Storage. *Angew. Chem., Int. Ed.* **2011**, *50*, 1683–1687.
42. Pech, D.; Brunet, M.; Durou, H.; Huang, P.; Mochalin, V.; Gogotsi, Y.; Taberna, P.-L.; Simon, P. Ultrahigh-Power Micrometre-Sized Supercapacitors Based on Onion-like Carbon. *Nat. Nanotechnol.* **2010**, *5*, 651–654.
43. Gao, W.; Singh, N.; Song, L.; Liu, Z.; Reddy, A. L. M.; Ci, L.; Vajtai, R.; Zhang, Q.; Wei, B.; Ajayan, P. M. Direct Laser Writing of Micro-Supercapacitors on Hydrated Graphite Oxide Films. *Nat. Nanotechnol.* **2011**, *6*, 496–500.
44. Mora-Sero, I.; Fabregat-Santiago, F.; Denier, B.; Bisquert, J.; Tena-Zaera, R.; Elias, J.; Levy-Clement, C. Determination of Carrier Density of ZnO Nanowires by Electrochemical Techniques. *Appl. Phys. Lett.* **2006**, *89*, 203117.
45. Fan, J.; Shavel, A.; Zamani, R.; Fábrega, C.; Rousset, J.; Haller, S.; Güell, F.; Carrete, A.; Andreu, T.; Arbiol, J.; *et al.* Control of

the Doping Concentration, Morphology and Optoelectronic Properties of Vertically Aligned Chlorine-Doped ZnO Nanowires. *Acta Mater.* **2011**, *59*, 6790–6800.
46. Myong, S. Y.; Lim, K. S. Highly Stable and Textured Hydrogenated ZnO Thin Films. *Appl. Phys. Lett.* **2003**, *82*, 3026–3028.
47. Dong, S.; Chen, X.; Gu, L.; Zhou, X.; Li, L.; Liu, Z.; Han, P.; Xu, H.; Yao, J.; Wang, H.; *et al.* One Dimensional MnO_2/Titanium Nitride Nanotube Coaxial Arrays for High Performance Electrochemical Capacitive Energy Storage. *Energy Environ. Sci.* **2011**, *4*, 3502–3508.
48. Liu, R.; Duay, J.; Lee, S. B. Redox Exchange Induced MnO_2 Nanoparticle Enrichment in Poly(3,4-ethylenedioxythiophene) Nanowires for Electrochemical Energy Storage. *ACS Nano* **2010**, *4*, 4299–4307.
49. Lu, X.; Yu, M.; Wang, G.; Zhai, T.; Xie, S.; Ling, Y.; Tong, Y.; Li, Y. H-TiO_2@MnO_2//H-TiO_2@C Core−Shell Nanowires for High Performance and Flexible Asymmetric Supercapacitors. *Adv. Mater.* **2013**, *25*, 267–272.
50. Lee, J. W.; Hall, A. S.; Kim, J.-D.; Mallouk, T. E. A Facile and Template-Free Hydrothermal Synthesis of Mn_3O_4 Nanorods on Graphene Sheets for Supercapacitor Electrodes with Long Cycle Stability. *Chem. Mater.* **2012**, *24*, 1158–1164.
51. El-Kady, M. F.; Strong, V.; Dubin, S.; Kaner, R. B. Laser Scribing of High-Performance and Flexible Graphene-Based Electrochemical Capacitors. *Science* **2012**, *335*, 1326–1330.
52. Yu Jin, K.; Haegeun, C.; Chi-Hwan, H.; Woong, K. All-Solid-State Flexible Supercapacitors Based on Papers Coated with Carbon Nanotubes and Ionic-Liquid-Based Gel Electrolytes. *Nanotechnology* **2012**, *23*, 065401.
53. Wee, G.; Salim, T.; Lam, Y. M.; Mhaisalkar, S. G.; Srinivasan, M. Printable Photo-Supercapacitor Using Single-Walled Carbon Nanotubes. *Energy Environ. Sci.* **2011**, *4*, 413–416.
54. Pan, C.; Guo, W.; Dong, L.; Zhu, G.; Wang, Z. L. Optical Fiber-Based Core−Shell Coaxially Structured Hybrid Cells for Self-Powered Nanosystems. *Adv. Mater.* **2012**, *24*, 3356–3361.
55. Guo, W.; Xue, X.; Wang, S.; Lin, C.; Wang, Z. L. An Integrated Power Pack of Dye-Sensitized Solar Cell and Li Battery Based on Double-Sided TiO_2 Nanotube Arrays. *Nano Lett.* **2012**, *12*, 2520–2523.